6

Radiofrequency Plasma Sources for Semiconductor Processing

Francis F. Chen

6.1
Introduction

In the etching and deposition steps in the production of semiconductor chips, plasma processing is required for three main reasons. First, electrons are used to dissociate the input gas into atoms. Second, the etch rate is greatly enhanced by ion bombardment, which breaks the bonds in the first few monolayers of the surface, allowing the etchant atoms, usually Cl or F, to combine with substrate atoms to form volatile molecules. And third, most importantly, the electric field of the plasma sheath straightens the orbits of the bombarding ions so that the etching is anisotropic, allowing the creation of features approaching nanometer dimensions.

The plasma sources used in the semiconductor industry were originally developed by trial and error, with little basic understanding of how they work. To achieve this understanding, many challenging physics problems had to be solved. This chapter is an introduction to the science of radiofrequency (rf) plasma sources, which are by far the most common. Sources operating at zero or other frequencies, such as 2.45 GHz microwaves, lie outside our scope. Most rf sources use the 13.56 MHz industrial standard frequency. Among these, there are three main types: (1) capacitively coupled plasmas or CCPs, also called reactive ion etchers (RIEs); (2) inductively coupled plasmas (ICPs), also called transformer coupled plasmas (TCPs); and (3) helicon wave sources, which are new and can be called HWSs.

6.2
Capacitively Coupled Plasmas

The principal parts of a CCP are shown schematically in Fig. 6.1. In its simplest form, the rf voltage is applied across two parallel metal plates, generating an oscillating electric field between them. This field accelerates electrons, heating their thermal distribution to have enough high-energy electrons in the tail to cause an ionization avalanche. The density rises to an equilibrium value set by the rf power and the density of the neutral gas. The silicon wafer to be processed is attached to the normally grounded electrode by an
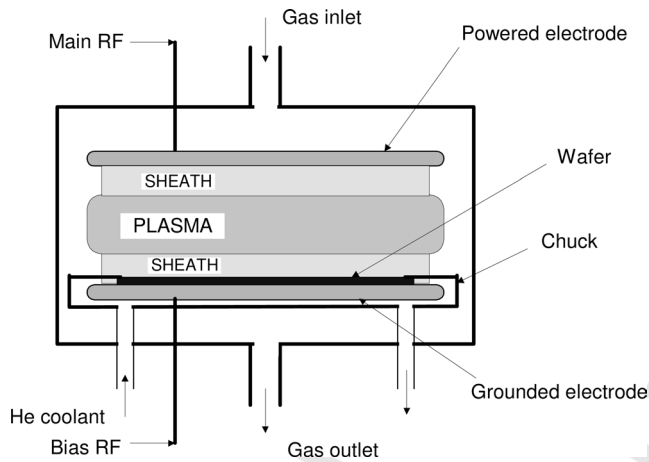
Fig. 6.1 Schematic of a capacitive discharge.

electrostatic chuck. The latter uses electrostatic charges to hold the wafer in contact with the electrode and also provides small channels for flow of helium to cool the wafer. To keep the plasma neutral, sheaths automatically form next to the electrodes providing an electric field (E-field) perpendicular to their surfaces. The potential drop in the sheath repels the fast-moving electrons so that they can escape no faster than the ions. At the same time, the sheath E-field accelerates the ions to bombard the surface and perform the beneficial functions mentioned above.

The sheath drop is of order $5KT_e$, where T_e is the electron temperature. For a 3 eV plasma, the ion energy is of order 15 eV. Since rf voltage is applied, the sheath drop and sheath thickness will oscillate at the rf frequency. Even if one electrode is grounded, the plasma potential will oscillate so as to make the two sheaths identical, but out of phase. The sheath oscillation will affect the ion energy distribution function (IEDF), depending on the transit time of the ions through the sheath. At low pressures, the IEDF at the wafer surface tends to be bimodal, with peaks at the maximum and minimum sheath drops, since a sine wave changes slowly at its extrema. CCPs are relatively inefficient ionizers and work best at high pressures and low densities. The sheath thickness, therefore, can become measurably large, of order millimeters. If the ion mean free path (mfp) for collisions with neutrals is smaller than the sheath thickness, the IEDF will be pressure-broadened. There are also other heating mechanisms. In resonant heating, some fast electrons can travel between the two sheaths without colliding, and those with just the right velocity can catch each sheath in its expanding phase, thus getting accelerated at each bounce. Such effects in classic CCPs are further described in textbooks [1,2].

6.2.1
Dual-Frequency CCPs

If ion bombardment energies larger than the normal sheath drop are desired, one can apply a second rf source, a *bias oscillator*, to the electrode bearing the substrate.

1   This is usually at a lower frequency, which has a larger effect on the massive ions. The
2   time-averaged sheath drop will then increase by the following rectification effect.
3   When the electrode is driven positive, a large electron current flows to it through the
4   lowered Coulomb barrier, but when the electrode goes negative, there is no
5   corresponding ion current because the ions are much slower. Unless the electrode
6   emits electrons, it will accumulate a negative charge. Applying a large rf bias voltage
7   to the substrate will, therefore, increase the dc (direct current) sheath drop even
8   though the bias voltage is ac. It is not generally possible to apply a dc voltage directly,
9   since parts of the wafer may be non-conducting. An rf voltage, however, will be
10   conveyed capacitively through these insulating layers.

11   Bias power supplies have been used for many years, but recently the dual-
12   frequency concept has found an important application in CCPs with extremely thin
13   gaps. These new devices perform well in oxide etch; that is, in the etching of SiO_2, a
14   difficult process since Si intrinsically etches faster than its oxide. The reason that thin-
15   gap CCPs work is not yet understood, but interest in them has spawned computa-
16   tional studies which have advanced the science of CCPs in general. Figure 6.2 shows a
17   schematic of this type of source. The electrodes are asymmetric; the wafer-bearing
18   plate is smaller to enhance the sheath drop there. The high frequency produces the
19   plasma, and the low frequency controls the ion distribution in the sheath. These
20   devices are quite different from the original RIEs because they operate at high
21   pressure (10–100 mtorr), and the gaps are very small (1–3 cm). With high rf bias
22   voltage, the sheaths are quite thick and can occupy most of the volume, leaving only a
23   small region of quasineutral plasma near the midplane. In this limit, what happens in
24   the sheath controls the plasma production. Upon striking the substrate, those
25   electrons that have penetrated the sheath produce more electrons by secondary
26   emission. The emitted electrons are then accelerated toward the plasma by the sheath
27   field. They ionize the neutral gas inside the sheath, since the ionization mfp can be
28   smaller than the sheath thickness. The avalanche that creates the plasma then starts
29   in the sheath.

30   Since the sheaths oscillate at two frequencies and their beats and harmonics, it is
31   clear that extensive computer simulation is required to model the complicated
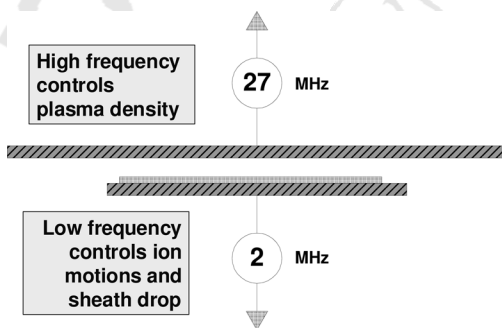
Fig. 6.2 Schematic of a thin-gap, dual-frequency CCP.

behavior in these collisional sheaths. We quote here just a few results from Lee's group at Pohang University in South Korea [3,5]. It is well known [1] in CCPs that the density increases with the square of the frequency. At constant power, therefore, the density increases, and the Debye length decreases, with frequency. The resulting change in sheath thickness is clearly demonstrated in Fig. 6.3. The IEDFs and EEDFs change not only with frequency but also with pressure. The pressure variation of IEDF is shown in Fig. 6.4, where it is seen that the typical bimodal distribution at low pressure is smoothed out by collisions at high pressure. Particle-in-cell simulations are invaluable in understanding complicated plasmas such as these. However, some aspects, such as why CCPs create less damage to oxide layers in etching, are still beyond the capabilities of theory. At this point, CCPs have been revived both as important manufacturing tools and as academically interesting subjects.
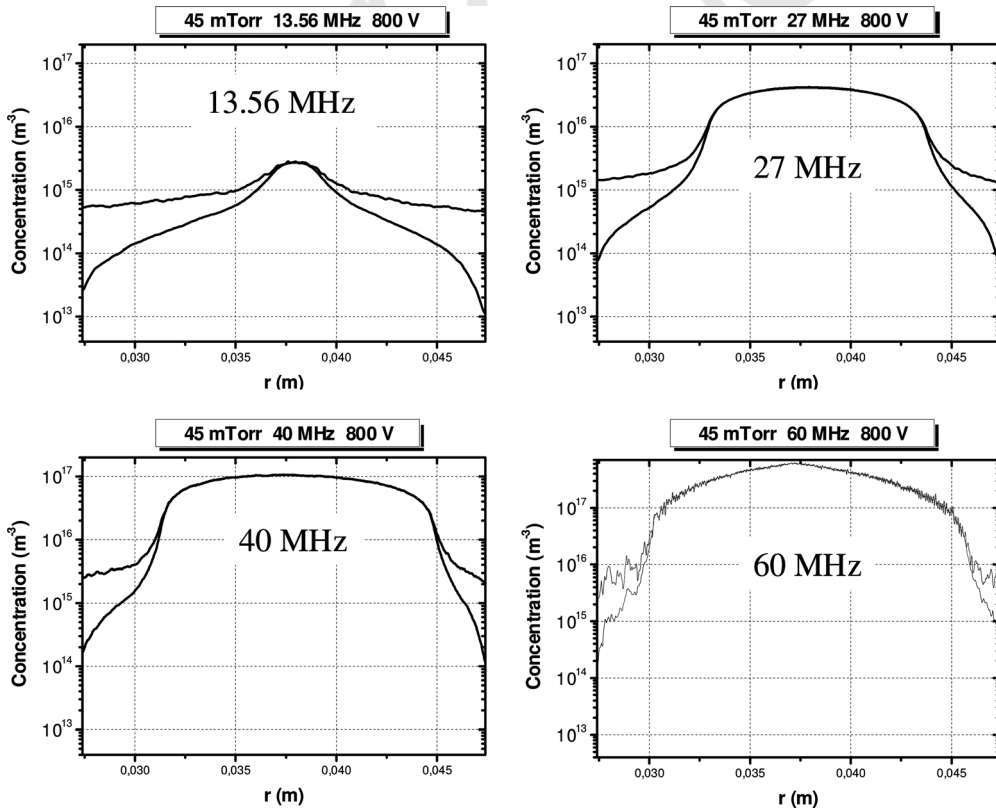
Fig. 6.3 Simulation of ion and electron density profiles at various frequencies [5].
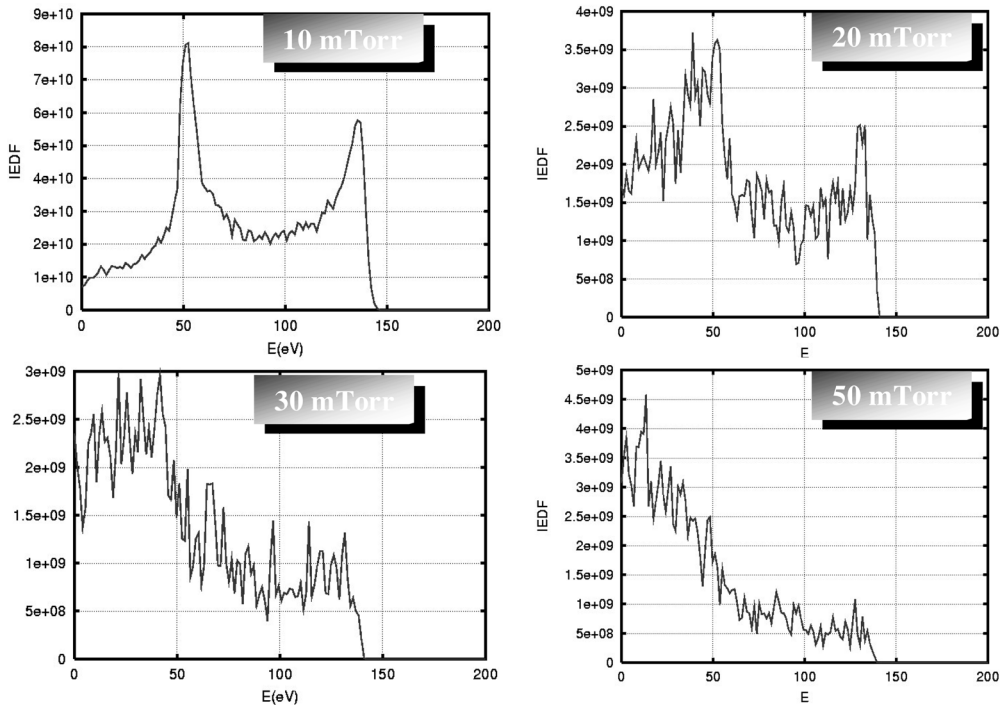
Fig. 6.4 Ion distributions at the substrate for different pressures [3].

6.3
Inductively Coupled Plasmas

6.3.1
General Description

Though simple and inexpensive, the original CCPs had a number of disadvantages, and a new generation of plasma sources was called for. For instance, the internal electrodes in CCPs introduced unnecessary impurities into the plasma. Until dual-frequency CCPs were introduced, there was a lack of control: changing the rf power changed both the plasma density and the sheath drop, and varying the pressure to do this would also change the chemistry. The high pressures also created a dust problem: negatively charged particulates of micrometer size or larger would form and be suspended above the substrate by the electric field, and these would collapse onto the wafer at plasma turn-off, thus destroying some of the chips. These problems are overcome in ICPs, which use an external coil (''antenna'') to induce an electric field inside the chamber according to Faraday's law. The most common antenna shapes are illustrated in Fig. 6.5.

(a)   (b)   (c)
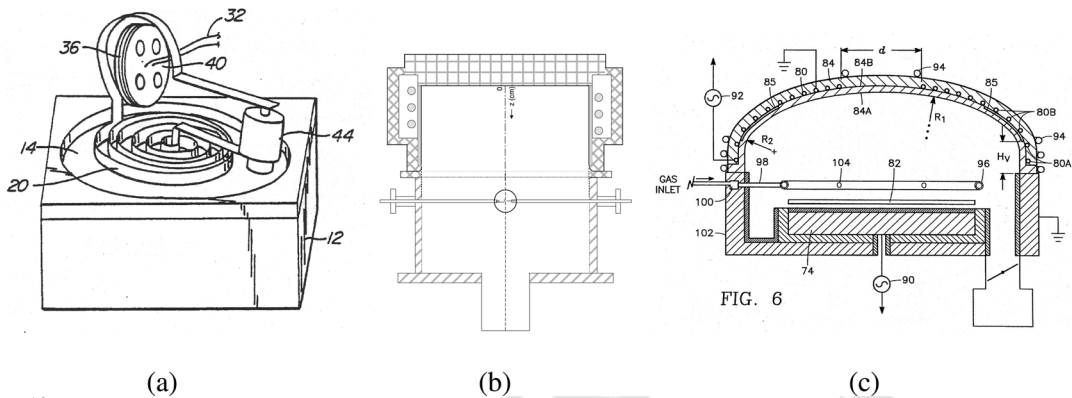
Fig. 6.5 Three types of ICP antennas: (a) planar coil; (b) cylindrical coil; (c) dome shaped.

Figure 6.5(a) shows the original Lam patent [6] for the TCP, whose antenna is a spiral coil, shaped like a stove-top heating element, separated from the plasma by a thick insulating plate. The diagram shows a variable transformer for impedance matching, giving the TCP its name. A capacitive automatch circuit is now standard. In Fig. 6.5(b), the antenna is a coil around the periphery of a cylindrical chamber. This type of antenna was successfully developed by the Plasma-Therm division of Unaxis. Figure 6.5(c) shows a patent from Applied Materials [7], the largest plasma source manufacturer. Its antenna is dome-shaped, combining the features of the previous two antennas, and has provision for adding a side coil also.

When an rf current is applied to a planar coil, an oscillating magnetic field (B-field) is created both above and below it. This generates a primarily azimuthal rf electric field. Inside the vacuum chamber, this E-field starts an electron avalanche which creates the plasma. Once the plasma is there, an electron current flows in a skin layer in the direction opposite to the current in the antenna and shields the plasma from the applied field. Thus, most of the rf energy is deposited within a skin depth of the surface. The plasma created there drifts downwards and decays while doing so. To be exposed to a large density, the substrate has to be placed not too far away from the top surface; but if it is too close, the plasma will be nonuniform because the discreteness of the antenna straps will be felt. There could be a problem with capacitive coupling if high voltages are applied at the ends of the antenna, and standing-wave effects can cause nonuniformity if the coil length is an appreciable fraction of the rf wavelength. These problems can be engineered away, and the TCP has been a very successful ICP.

To see how the design of the TCP coil could affect the plasma uniformity, one can compute the B-field lines induced. This is shown in Fig. 6.6, where the spirals have been approximated by circular rings. Figure 6.6(a) and (b) compare three rings with two rings: the field shapes are almost identical. Figure 6.6(a) and (c) compare copper

(a)   (b)

(c)   (d)
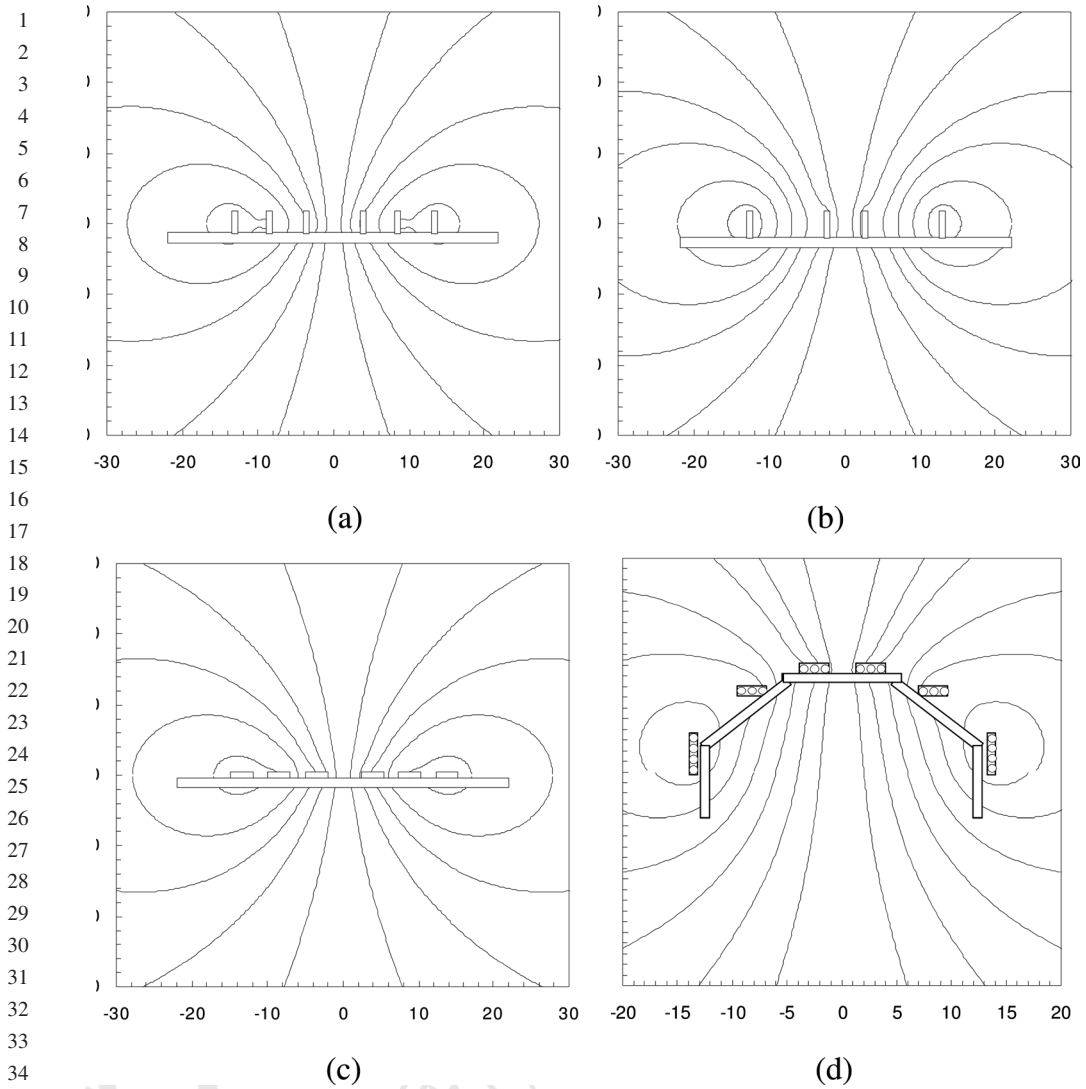
Fig. 6.6 Magnetic field patterns of ICP antennas: (a) three circular rings; (b) two rings; (c) three rings lying flat; (d) rings arranged on a dome.

strips standing on end with those lying flat. Though the field shapes are almost the same, they are centered at the mid-height of the strips. Thus, flat conductors bring the strong-field region closer to the plasma. Figure 6.6(d) shows the pattern created by an antenna placed on a dome. It is quite different from the others; the lines diverge less rapidly below the coils, possibly leading to more uniform ionization. This type of ICP is manufactured by Applied Materials.

6.3.2
Anomalous Skin Depth

At first glance, the side-wound antenna of Fig. 6.5(b) should give poor plasma uniformity. Since the skin depth is of the order of a few centimeters, much less than the radius of the substrate to be processed, one would expect the density to be high only near the periphery. Actually, the opposite is true, and parameters can be adjusted to have excellent uniformity across the wafer. Radial profiles of $n(r)$, $T_e(r)$, and the rf field $B_z(r)$ are shown in Fig. 6.7. The rf field decays away from the wall with a skin depth of about 3 cm, and T_e peaks in the skin layer, as expected. However, the density actually peaks near the axis. How does plasma get created where there is no power deposition? This problem, called *anomalous skin depth*, has been known since the 1970s and has received much attention from theorists. Their favorite argument is that fast electrons accelerated in the skin layer can wander into the interior of the discharge by their thermal motions. These theories, which have been summarized [9], are usually linear, kinetic, and in Cartesian geometry. By following the orbits of electrons during many rf cycles, we have shown [8] that this fortuitous effect is caused by a combination of cylindrical geometry and the nonlinear Lorentz force $\mathbf{F}_L = -e\mathbf{v} \times \mathbf{B}_{rf}$. Figure 6.8 shows two orbits of an electron starting at rest in the skin layer as the rf field varies over four cycles. One orbit is computed including $\mathbf{F}_L$, and the other without it. The electron is accelerated in the azimuthal E-field and is reflected specularly from the Debye sheath at the wall. It makes glancing collisions with the wall and does not wander into the interior of the discharge until it has slowed down below ionizing velocities. The Lorentz force due to $v_\theta \times B_z$ is in the radial
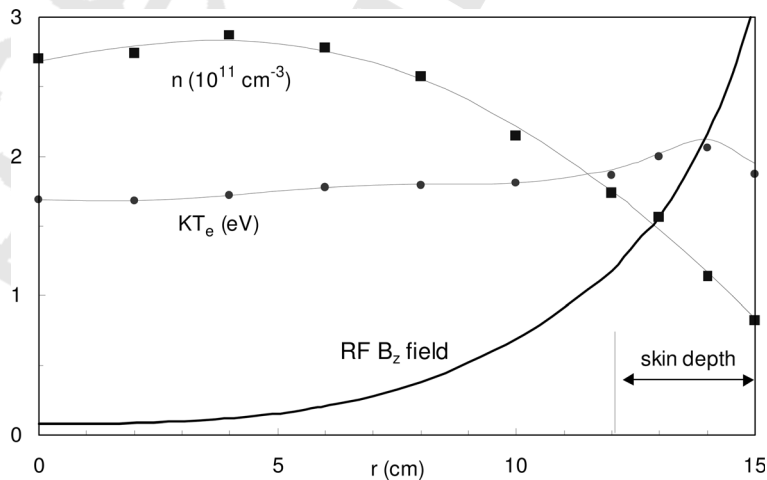
Fig. 6.7 Measurements in a side-fed ICP of plasma density, electron temperature, and rf field strength vs. radius [8].
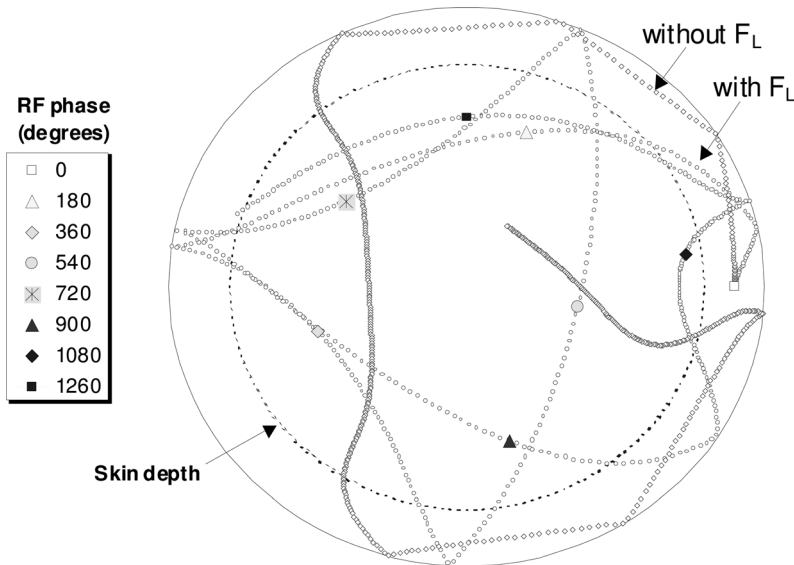
Fig. 6.8 Paths of an electron starting in the skin layer, through the first four rf cycles, with and without the Lorentz force.

direction and causes the electrons to collide with the wall at steeper angles, bringing them more rapidly into the center, while they still have ionizing energies. When F_L is included, $n(r)$ actually peaks near the axis, in agreement with Fig. 6.7, due to two effects: (a) orbits crossing the discharge tend to raise the density in the interior because of the smaller volume there, and (b) electrons created near the center spend a long time there before reaching the skin layer where they can gain energy. The puzzle of anomalous skin depth would appear to be solved, but further computations including particle motion in the axial direction need to be done. In any case, how ICPs actually work is not a simple problem.

6.3.3
Magnetized ICPs

In the field patterns of Fig. 6.6, it is clear that half the magnetic field energy appears above the antenna and is not utilized. This field is partly canceled by the skin current in the plasma, but the reduction is not large because the skin current is farther away and is diffuse. To channel that energy into the plasma, Colpo and co-workers [10] have modified ICPs by covering the antenna with a magnetic material. The mechanism is sketched in Fig. 6.9. The magnetization vector **H** is unaffected by the permeability μ and is the same in both parts of the diagram. When a high-μ ferrite material is added to the antenna, the field $\mathbf{B} = \mu\mathbf{H}$ is greatly enhanced, effectively capturing the magnetic energy which is normally lost and injecting it back into the plasma. Further details can be found in Chapter 2.

$$\nabla \times H = J$$
$$B = \mu H$$
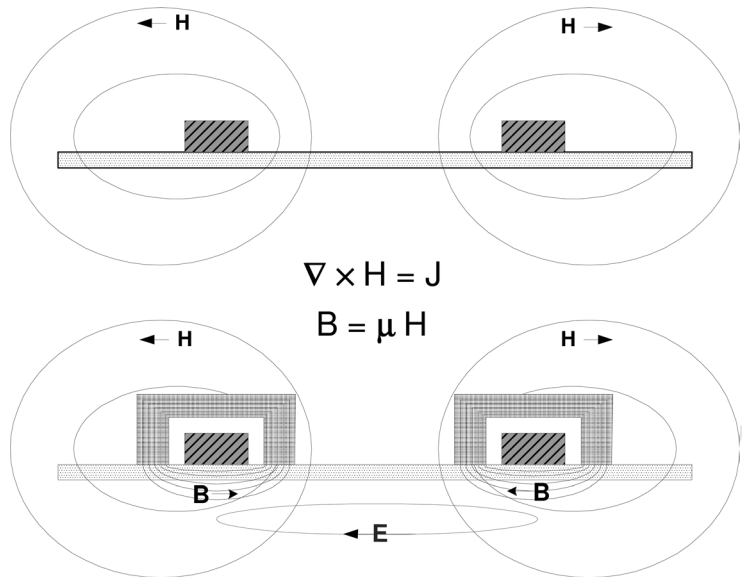
Fig. 6.9 Schematic of magnetic field lines of an ICP antenna before and after modification with ferromagnetic material.

To cover large areas, ICP antennas can consist of parallel rods connected in various series–parallel combinations. The device of Meziani and co-workers [10,11] is shown in Fig. 6.10. It is found that the magnetic cover increases not only the rf field but also the plasma uniformity. Lee *et al*. [12–15] have also used various serpentine antennas, with permanent magnets placed in pairs above the antenna (Fig. 6.11). A physical picture of the resulting fields and their effect has not been given, but these configurations have been modeled in detail by Park *et al*. [16]. Though ICPs are standard in the semiconductor industry, they are being further developed for large-area display applications by the use of magnetic materials.
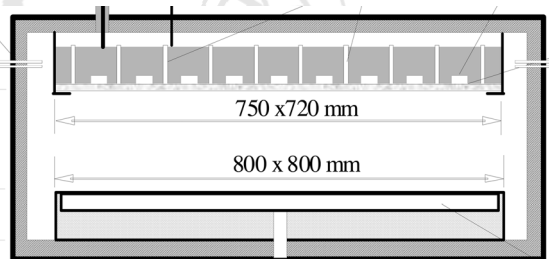
Fig. 6.10 Processing chamber with a magnetized array of linear ICP antennas [11].

1
2
3
4
5
6
7
8
9
10
11
12
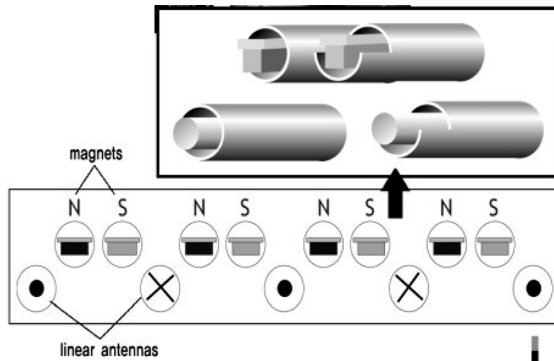
Fig. 6.11 ICP enhanced with permanent magnets above the antenna legs, all encased in quartz tubes (G.Y. Yeom, personal communication).

6.4
Helicon Wave Sources

6.4.1
General Description

This type of plasma source was discovered by Boswell [17] in 1970, and its wave nature was verified in 1984 [18]. As in an ICP, an antenna, an rf power source, and a matching circuit are used; but a dc magnetic field is added. In the presence of this B_0-field, the antenna launches circularly polarized *helicon* waves, related to ''whistler'' waves in the ionosphere, along $\mathbf{B}_0$. For reasons not known for over a decade, these waves are very efficient ionizers, producing plasma densities well over $10^{19}\,\mathrm{m}^{-3}$ with only a kilowatt of rf power. Helicon sources differ from CCPs and ICPs in several essential ways. First, they are more complicated because of the dc B-field. Second, they can generate plasma densities an order of magnitude higher than previous devices with the same power. And third, they were studied and understood before widespread acceptance by industry.

Figure 6.12 shows a typical apparatus for studying the propagation of helicon waves and the nature of the plasmas created. A commercial helicon source [19] is shown in Fig. 6.13. This device uses two ring antennas with opposite currents, and the magnetic field shape is controlled with the current ratio in two coils, one enclosing the other, also carrying opposite currents. These $m = 0$ antennas, where m is the azimuthal symmetry number, are less common than $m = 1$ antennas, of which two are shown in Fig. 6.14. The Nagoya III antenna is symmetric and launches both right-hand (RH) and left-hand (LH) circularly polarized waves in both directions. The HH antenna is a half-wavelength long and is meant to match the helicity of the helicon wave. It launches RH waves in one direction and LH waves in the other, the directions reversing with the $\mathbf{B}_0$ field. The most efficient coupling is with bifilar antennas (two HH antennas 90° apart in azimuth, also phased 90° apart in time, giving a field that rotates with the helicon wave [20].
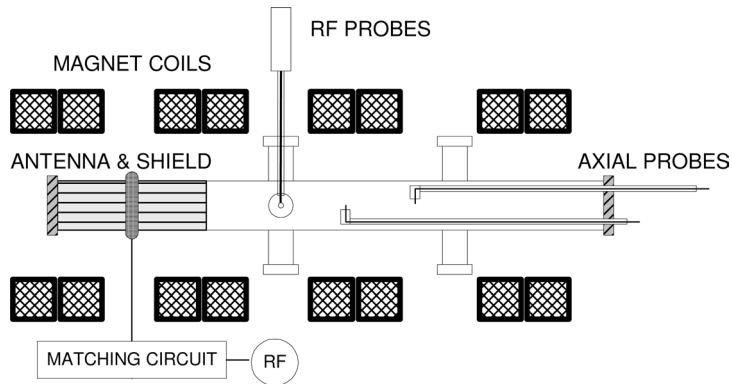
Fig. 6.12 Typical experimental setup for studying helicon waves.

6.4.2
Unusual Features

Many challenging problems have arisen in the behavior of helicon discharges, and these have been solved one by one. When either the rf power or the magnetic field is increased after breakdown, the plasma density increases not continuously but by
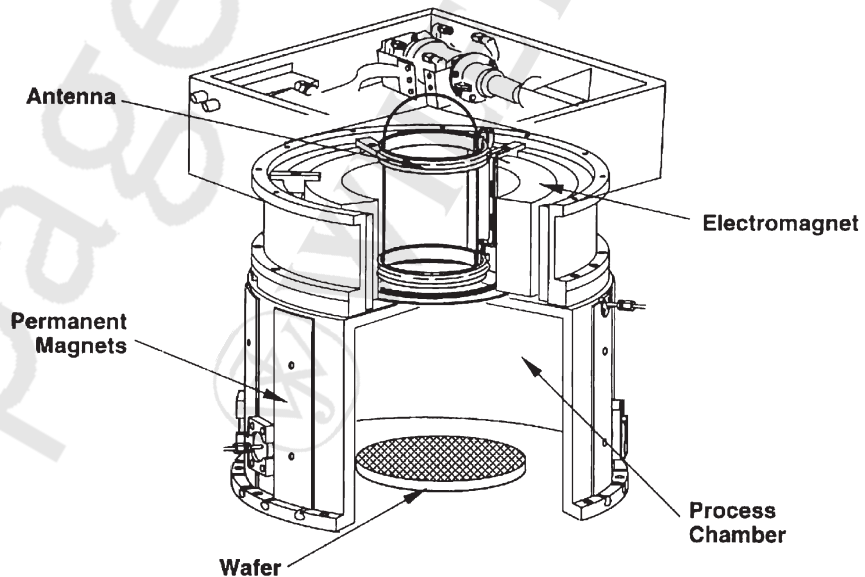
Fig. 6.13 The PMT MØRI device, a commercial reactor with two coplanar magnetic coils at the source and with multi-dipole confinement with permanent magnets in the processing chamber. The cut-away box at the top is the matching circuit [19].
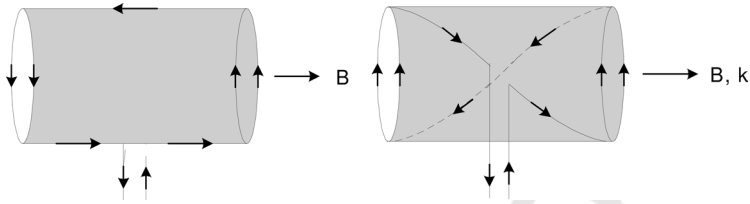
Fig. 6.14 Two common helicon antennas: a Nagoya Type III antenna (left) and a half-helical (HH) antenna (right).

discrete jumps. At low power, the coupling is capacitive, and the discharge is a CCP. As the power is raised, the plasma jumps into ICP operation as inductive coupling takes hold. When the conditions for propagation of helicon waves are met, there is a large jump into the lowest helicon mode and the peak density can be 20 times higher than in ICP mode. There may be further jumps into higher-order radial modes. A second observation is that the density peaks, not under the antenna, but many centimeters downstream from it, as shown in Fig. 6.15. There are three possible reasons for this. First, as seen from the T_e curve, the temperature decays downstream because of inelastic collisions (line radiation and ionization). Second, plasma is ejected from the antenna region with a drift velocity comparable to the ion acoustic
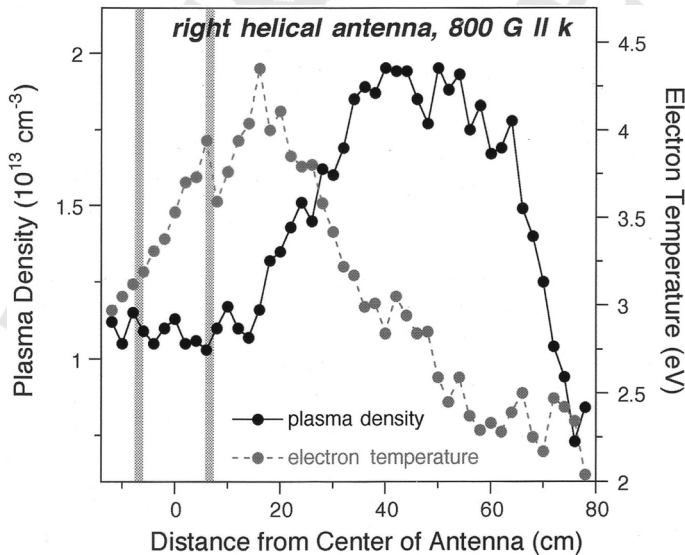
Fig. 6.15 Plasma density $n(z)$ and temperature $KT_e(z)$, where z is the direction of $\mathbf{B}_0$. The antenna is located between the vertical bars.

velocity c_s. This is just the Bohm criterion for sheath formation. There is no sheath here, but the criterion still has to be met if there are very few ions created downstream which can travel back to the antenna. Finally, there may actually be a little ionization downstream due to parametric instabilities, an effect recently verified in experiment. The result is that the helicon discharge is an ideal ''remote'' source, in which the substrate can be located in a desirable region of high density and low T_e, far from the high fields near the antenna.

A second, more important, problem is: What causes the high ionization efficiency of HWSs compared with ICPs? There is no difference in confinement, since the B-fields of 50–1000 Gs (5–100 mT) normally used are not sufficient to confine the ions, and the electrons are not confined axially. Hence, the difference must be in the way in which rf energy is absorbed. In ICPs, collisional absorption converts the electron energy gained in the skin layer into a general rise in KT_e, and the tail of this Maxwellian distribution does the ionization. Since helicon waves travel along $\mathbf{B}_0$ with velocities comparable to those of 100 eV electrons, could they not trap electrons and accelerate them by Landau damping? This mechanism was suggested by Chen [21], and several groups have indeed detected the fast electrons indicative of this process. However, these electrons were too few in number to account for the increased ionization, and this hypothesis was later disproved [22]. Meanwhile Shamrai et al. [23] suggested a new absorption mechanism; namely mode conversion to Trivelpiece–Gould (TG) modes at the boundary. The TG mode, essentially an electrostatic electron cyclotron wave in a cylinder, is needed to satisfy the radial boundary conditions. The helicon wave itself is weakly damped by collisions, but it transfers its energy to the TG wave, which is rapidly damped as it propagates slowly inward from the boundary. Computations by Arnush [24] have confirmed the dominance of this absorption process. TG modes are difficult to detect, however, because they only occur in a thin layer at the wall; however, by using a low B-field to widen this layer and developing an rf current probe, Blackwell et al. [25] verified the existence of this mechanism.

An efficient absorption mechanism increases the plasma resistance R_p, and therefore a greater fraction of the rf energy is deposited in R_p rather than in the parasitic resistances R_c in the matching circuit and connections. If $R_p/R_c >> 1$, there would be no advantage of higher R_p/R_c. In ICPs with $n \leq 10^{18}$ m^{-3}, however, R_p/R_c is small enough that increasing it by operating in the helicon mode would deposit more energy into the plasma. The large densities $\geq 10^{19}$ m^{-3} in the helicon's ''Big Blue Mode'' are a different matter. The density is high and fully ionized only in a central core; the more uniform deposition with TG modes at the edge is not seen. We believe that in this case there is an ionization instability, in which neutrals are depleted near the axis, and this allows T_e to rise and the ionization rate to grow exponentially.

In free space, the whistler wave is known to propagate only when it is RH polarized. Helicons, however, are in a bounded medium, and it is easily shown that both RH and LH polarizations are possible. It was unexpected that only the RH mode is strongly excited in practice; the LH mode hardly exists. A helical antenna is therefore highly directional and launches helicon waves only in the direction dictated by the sign of its helicity and the direction of $\mathbf{B}_0$. Computations confirm this, but the physical

explanation of this effect is not simple. The LH wave has a somewhat smaller amplitude at the edge than the RH wave does. Perhaps this causes the coupling to the TG mode to be much weaker.

A final puzzle we can mention is that of the low field peak: the density is found to have a small peak at low B-fields of the order of 10–100 Gs (1–10 mT), whereas it should increase linearly with $\mathbf{B}_0$. Computations have shown [26] that this peak is caused by constructive interference by the helicon wave reflected from a back plate and occurs only with bidirectional antennas. This effect can be used to design more economical helicon reactors using low fields. Most of these advances in understanding were made with simple geometries and uniform B-fields. To model a realistic reactor such as that shown in Fig. 6.13 would require extensive computer simulations. Several of these have been done, and these have shown that features such as the downstream density peak and TG modes actually play a role even in complex geometries.
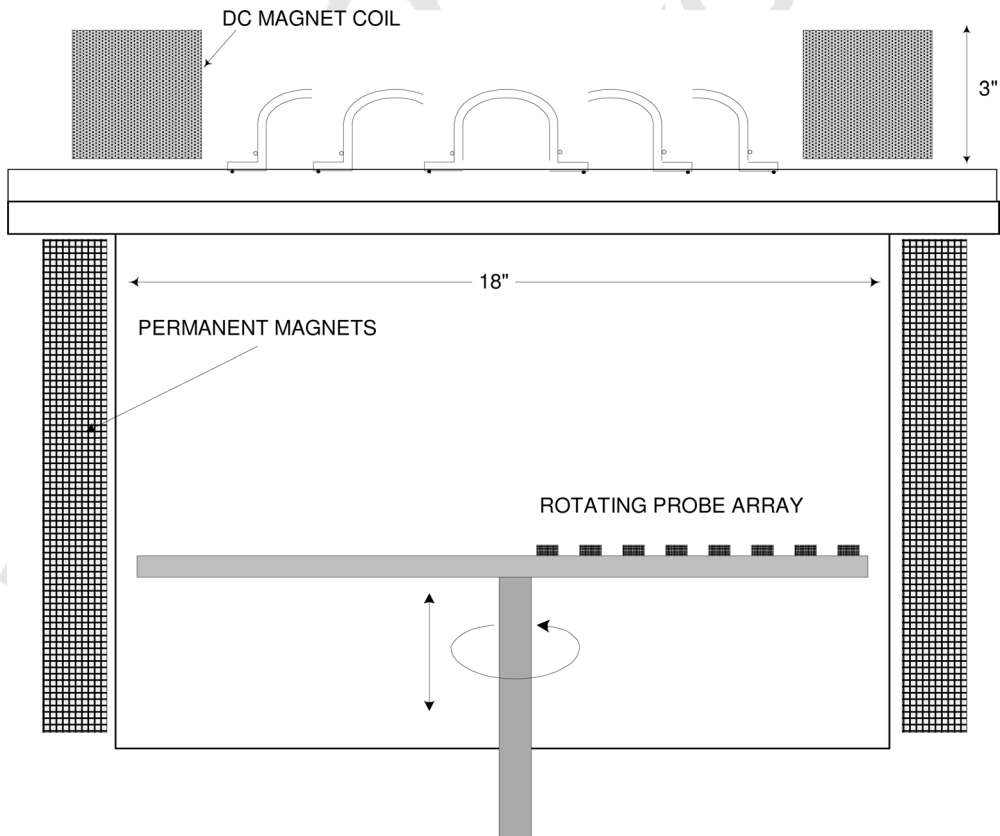
Fig. 6.16 Seven-tube array of helicon sources with a large electromagnet.
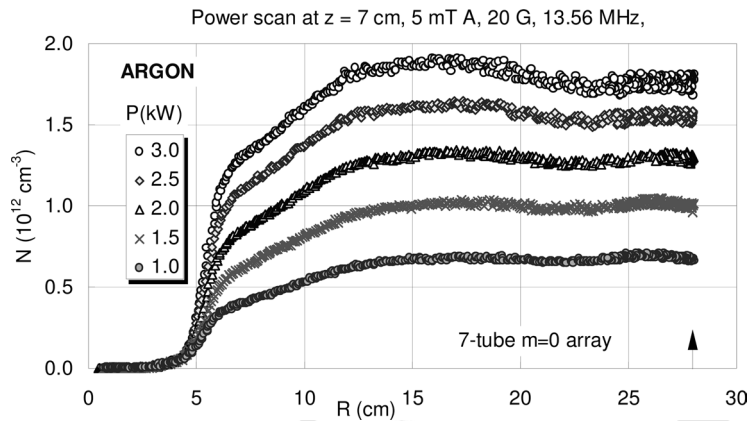
Fig. 6.17 Density profiles $n(r)$ at various rf powers in argon, 7 cm below the distributed source of Fig. 6.16.

6.4.3
Extended Helicon Sources

As in the case of ICPs, helicon sources can also be extended to cover large areas. This can be done with serpentine antennas [27] or with multiple small tubes. Figure 6.16 shows a distributed source arrayed with one tube surrounded by six others [28]. Each tube is very short, with a simple $m = 0$ antenna; and a single large magnet coil surrounds the array. Figure 6.17 shows density profiles at various rf powers. With a total power of 3 kW, a plasma uniform to $\pm 3\%$ can be created 7 cm below the sources with a density of nearly 10^{18} cm^{-3} over a 400 mm diameter substrate.

In summary, the study of plasma sources has not only played an essential role in the production of semiconductor chips but has also provided challenging problems for the academic community to solve. The standard CCP and ICP sources are being extended and modified for new applications, and the new helicon sources are a promising prospect for the next generation of etching and deposition reactors.

References

1 Lieberman, M.A. and Lichtenberg, A.J. (2005) *Principles of Plasma Discharges and Materials Processing*, 2nd edn , Wiley-Interscience, Hoboken, NJ.

2 Chen, F.F. and Chang, J.P. (2003) *Principles of Plasma Processing*, Kluwer Academic/Plenum Publishers, New York.

3 Lee, J.K., Babaeva, N.Yu., Kim, H.C., Manuilenko, O.V. and Shon, J.W. (2004) *IEEE Trans. Plasma Sci.*, **32**, 47.

4 Babaeva, N.Yu., Lee, J.K. and Shon, J.W. (2005) *J. Phys. D: Appl. Phys.*, **38**, 287.

5 Lee, J.K., Manuilenko, O.V., Babaeva, N.Yu., Kim, H.C. and Shon, J.W. (2005) *Plasma Sources Sci. Technol.*, **14**, 89.

6 US Patent 4,948,458, Lam Research (1990).

7 US Patent 4,948,458, Applied Materials (1993).

8 Evans, J.D. and Chen, F.F. (2001) *Phys. Rev. Lett.*, **86**, 5502.

9 Kolobov, V.I. and Economou, D.J. (1997) *Plasma Sources Sci. Technol.*, **6**, R1. For example.

10 Meziani, T., Colpo, P. and Rossi, F. (2001) *Plasma Sources Sci. Technol.*, **10**, 276.

11 Colpo, P., Meziani, T. and Rossi, F. (2005) *J. Vac. Sci. Technol. A*, **23**, 270.

12 Lee, Y.J., Han, H.R. and Yeom, G.Y. (2000) *Surf. Coat. Technol.*, **133**, 612.

13 Lee, Y.J., Kim, K.N., Song, B.K. and Yeom, G.Y. (2002) *Mater. Sci. Semicond. Process.*, **5**, 419.

14 Lee, Y.J., Kim, K.N., Song, B.K. and Yeom, G.Y. (2003) *Thin Solid Films*, **435**, 275.

15 Kim, K.N., Lee, Y.J., Kyong, S.J. and Yeom, G.Y. (2004) *Surf. Coat. Technol.*, **177**, 752.

16 Park, S.E., Cho, B.U., Lee, J.K., Lee, Y.J. and Yeom, G.Y. (2003) *IEEE Trans. Plasma Sci.*, **31**, 628.

17 Boswell, R.W. (1970) *Phys. Lett. A*, **33**, 457.

18 Boswell, R.W. (1984) *Plasma Phys. Control. Fusion*, **26**, 1147.

19 Tynan, G.R., Bailey, A.D., III, Campbell, G.A., Charatan, R., deChambrierA., Gibson, G., Hemker, D.J., Jones, K., Kuthi, A., Lee, C., Shoji, T. and Wilcoxson, M. (1997) *J. Vac. Sci. Technol. A*, **15**, 2885.

20 Miljak, D.G. and Chen, F.F. (1998) *Plasma Sources Sci. Technol.*, **7**, 61.

21 Chen, F.F. (1991) *Plasma Phys. Control. Fusion*, **33**, 339.

22 Blackwell, D.D. and Chen, F.F. (2001) *Plasma Sources Sci. Technol.*, **10**, 226.

23 Shamrai, K.P. and Sharanov, V.B. (1995) *Plasma Phys. Control. Fusion*, **36**, 1015. (1996) *Plasma Sources Sci. Technol*, **5**, 43.

24 Arnush, D. (2000) *Phys. Plasmas*, **7**, 3042.

25 Blackwell, D.D., Madziwa, T.G., Arnush, D. and Chen, F.F. (2002) *Phys. Rev. Lett.*, **88**, 145002.

26 Chen, F.F. (2003) *Phys. Plasmas*, **10**, 2586.

27 Jewett, R.F.Jr., (1995) PhD thesis, University of New Mexico.

28 Chen, F.F., Evans, J.D. and Tynan, G.R. (2001) *Plasma Sources Sci. Technol.*, **10**, 236.